Substituent effects on exchange anisotropy in single- and multiorbital organic radical magnets

Jonathan Marbey,[1,*] Aaron Mailman,[2] Richard T. Oakley,[3] Stephen Hill,[1,†] and Stephen M. Winter[4,‡]

[1]*National High Magnetic Field Laboratory and Department of Physics, Florida State University, Tallahassee, Florida 32310, USA*

[2]*Department of Chemistry, University of Jyväskylä, P.O. Box 35, Jyväskylä FI-40014, Finland*

[3]*Department of Chemistry, University of Waterloo, Waterloo, Ontario, Canada N2L 3G1*

[4]*Department of Physics, Wake Forest University, Winston-Salem, North Carolina 27109, USA*

(Received 24 September 2023; revised 18 March 2024; accepted 20 March 2024; published 19 April 2024)

The contribution of heavy-atom substituents to the overall spin-orbit interaction in two classes of organic radical molecular magnets is discussed. In "single-orbital" radicals, spin-orbit coupling (SOC) effects are well described with reference to pairwise anisotropic exchange interactions between singly occupied spin-bearing orbitals on neighboring molecules; anisotropy requires the presence of spin density on heavy-atom sites with principal quantum number $n > 3$. In "multiorbital" radicals, SOC involving virtual orbitals also contributes to anisotropic exchange and, as a result, the presence of heavy ($n > 3$) atoms in formally non-spin-bearing sites can enhance pseudodipolar ferromagnetic interaction terms. To demonstrate these effects, ferromagnetic and antiferromagnetic resonance spectroscopies have been used to probe the exchange anisotropy in two organic magnets, one a "single-orbital" ferromagnet, the other a "multiorbital" spin-canted antiferromagnet, both of which contain a heavy-atom iodine ($n = 5$) substituent. While the symmetry of the singly occupied molecular orbital in both radicals precludes spin-orbit contributions from iodine to the overall exchange anisotropy, the symmetry and energetically low-lying nature of the lowest unoccupied molecular orbital in the latter allows for appreciable spin density at the site of iodine substitution and, hence, a large exchange anisotropy.

DOI: 10.1103/PhysRevMaterials.8.044406

I. INTRODUCTION

The early development of organic (*p*-block) radical-based magnetic materials was characterized by low magnetic ordering temperatures (<2 K) and vanishingly small coercive fields ($H_c < 10$ Oe) [1–6]. Higher ordering temperatures were eventually encountered, for example, in the spin-canted antiferromagnet β-NCC_6F_4-DTDA ($T_N = 36$ K) [7] and the charge-transfer salt ferromagnets [BBDTA][$GaCl_4$] ($T_C = 7$ K) [8], [BBDTA][$Au(CN)_2$] ($T_C = 8$ K) [9], and C_{60} • TDAE ($T_C = 16$ K) [10], but in none of these materials was there any indication of magnetic hysteresis. In contrast to spin $S > \frac{1}{2}$ metal-based systems, where single-ion anisotropy may arise from crystal-field effects, Kramers' theorem forbids zero-field magnetic anisotropy for isolated $S = \frac{1}{2}$ radicals. In such systems, the source of coercivity is therefore confined to intermolecular spin-spin interactions, either through long-range dipolar effects or anisotropic spin-orbit coupling (SOC) contributions to the exchange. The former depends on crystal morphology and microscopic structure, the latter on the presence of heavy atoms (with principal quantum number $n > 3$) in spin-bearing sites. It is therefore not surprising that early "light-atom" magnets such as those noted above showed no coercive field, H_c, as SOC effects are very weak.

Evidence for increased magnetic hysteresis and possible spin-orbit-mediated anisotropic exchange interactions emerged with the development of resonance stabilized heterocyclic radicals based on the *N*-alkyl-pyridine bridged bisdithiazolyl framework and its selenium-containing variants **1A**–**1D** (E_1/E_2 = S/Se; see Fig. 1) [11–13]. From a structural perspective the effects of steric protection provided by the exocyclic substituents (R_1/R_2) coupled with a highly delocalized spin distribution was sufficient, in most cases [14], to preclude solid-state association (dimerization), even for selenium-based radicals. These features allowed for systematic studies of isotropic and anisotropic exchange between spins on heavy ($n > 3$) centers [15]. In one particular isostructural family of radicals, **1A**–**1D** (R_1 = Et, R_2 = Cl) with space group $P\bar{4}2_1m$, in which herringbone-packed arrays of slipped radical π stacks are wrapped about $\bar{4}$ axes (Fig. 2), ferromagnetic (FM) order was observed, with the critical temperature T_C increasing with the extent of Se incorporation from 12.8 K in **1B** to 17 K in **1D**, the latter being very high for an organic ferromagnet at ambient pressure [16,17]. Moreover, in both cases, significant and increasing magnetic hysteresis was observed, with the coercive field H_c rising from 250 Oe in **1B** (at 2 K) to 1370 Oe in **1D** (at 2 K). These values, which are two to three orders of magnitude larger than those encountered in conventional light-atom organic magnets, were proposed to arise from the contribution of SOC effects to anisotropic exchange occasioned by the incorporation of selenium; similar trends had been observed in the *g* anisotropy of isolated S- and Se-based radicals. Later ferromagnetic resonance (FMR) measurements of the magnitude of the magnetic anisotropy in **1B** and **1D** (R_1/R_2 = Et/Cl), both with and without applied pressure, supported this interpretation [18–20]. Subsequent work on the isostructural bromo derivative

*Present address: Laboratory for Physical Sciences, 8050 Greenmead Drive, College Park, MD 20740, USA.

†shill@magnet.fsu.edu

‡winters@wfu.edu

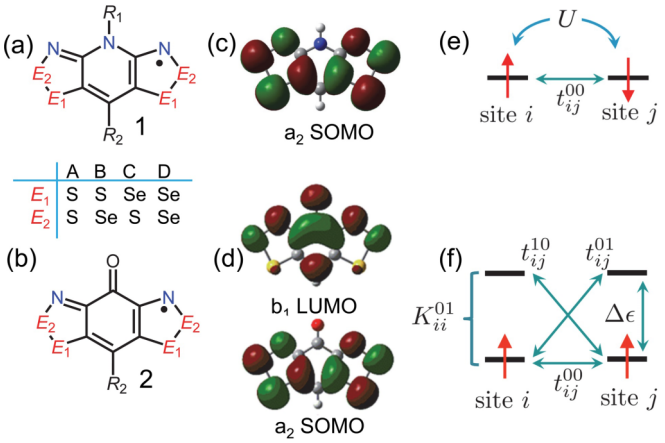

FIG. 1. Valence bond (VB) representations of (a) "single-orbital" and (b) "multiorbital" bisdithiazolyl radicals **1** and **2** and their selenium-containing variants. Kohn-Sham singly occupied molecular orbital (SOMO) for (c) prototypal model **1A** (R_1/R_2 = H) and (d) SOMO/LUMO pair for **2A** (R_2 = H). (e) Two-site, two-orbital interaction diagram for two adjacent radicals, **1**, expressing site-to-site exchange coupling, J_{ij}, in terms of the on-site Coulomb potential, U, and electron hopping, t_{ij}^{00}. (f) Two-site, four-orbital interaction diagram for two radicals, **2**, with a small SOMO-LUMO gap, $\Delta\epsilon$. The SOMO-SOMO (t_{ij}^{00}) and SOMO-LUMO (t_{ij}^{10} and t_{ij}^{01}) hopping integrals, and the SOMO-LUMO electron exchange integral, K_{ii}^{01}, are indicated [15].

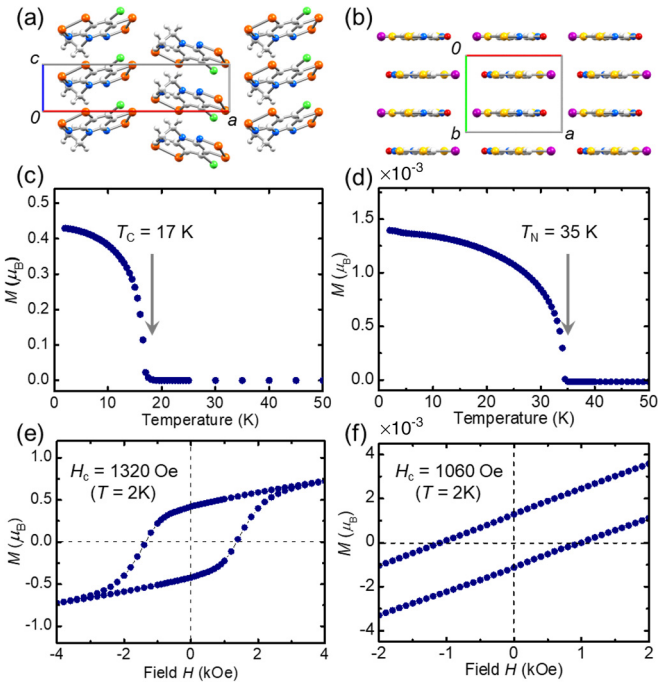

FIG. 2. (a) Herringbone packed arrays of slipped π stacks of **1D** (R_1/R_2 = Et/Cl), space group $P\bar{4}2_1m$, viewed parallel to the b axis [16]. (b) Head-over-tail packed layers of radicals in **2A**•EtCN (R_2 = I), space group *Pnma*, viewed parallel to the c axis [30]. (c) Magnetization M versus T at H = 100 Oe for **1D** (R_1/R_2 = Et/Cl) [16] and (d) for **2A**•EtCN (R_2 = I) [30]. Hysteresis in M versus H at T = 2 K for (e) **1D** (R_1/R_2 = Et/Cl) [16] and (f) **2A**•EtCN (R_2 = I) [30].

1D (R_1/R_2 = Et/Br) revealed a slight increase in H_c to 1620 Oe (at 2 K) [21], while in the iodo derivative **1D** (R_1/R_2 = Et/I), lower T_C (10.5 K) and H_c (370 Oe at 2 K) values were observed [22]. However, the T_C of all three materials (R_2 = Cl, Br, I) increased under pressure, reaching 27.5 K for R_2 = I at 2 GPa [23].

Synthetic routes to a second class of resonance stabilized bisdithiazolyl radical, **2A**, in which the *N*-alkyl-pyridine bridge in **1A** is replaced by an oxobenzene unit [Fig. 1(b)], were later developed. While the selenium-containing variants **2B**–**2D** are strongly associated in the solid state and therefore lack any magnetic signature, a wide range of all-sulfur radicals **2A** with different R_2 groups have been characterized, many of which display interesting magnetic as well as conductive properties [24–27]. In particular, the family of halogen-substituted radicals **2A** (R_2 = F, Cl, Br, I) has provided a rich source of magnetic information; several phases have been observed, including some solvates. Both the R_2 = F (space group $Cmc2_1$) [28] and R_2 = Cl (space group $Pna2_1$) [29] derivatives order as spin-canted antiferromagnets, with Néel temperatures T_N = 13 and 8 K, and coercivities H_c = 290 and 80 Oe (at 2 K), respectively. While the chloro, bromo, and iodo derivatives form isostructural acetonitrile (MeCN) solvates (space group $Pna2_1$) which do not order magnetically, crystallization of the iodo derivative from propionitrile (EtCN) generates a solvate **2A**•EtCN (R_2 = I), space group *Pnma*, which adopts a layered structure (Fig. 2) and orders as a spin-canted antiferromagnet (SCAFM) [30]. This latter material is striking not only for its high ordering temperature (T_N = 35 K), which is just below that of β-NCC$_6$F$_4$-DTDA [7], but also for its coercive field (H_c = 1060 Oe at 2 K), which is exceptionally large for a nominally light-atom radical.

Understanding the magnetic properties of these two classes of radicals **1** and **2**, in particular, the role played by heavy atoms ($n > 3$) in determining the degree of magnetic anisotropy that ultimately influences magnetic hysteresis, requires different theoretical models for describing anisotropic exchange interactions [15]. In class **1** radicals, which we refer to as "single-orbital" systems, pairwise anisotropic exchange arises due to the effects of SOC on the interactions between spin-bearing singly occupied molecular orbitals (SOMOs) on neighboring molecules; anisotropy requires the presence of spin density on heavy-atom sites with principal quantum number $n > 3$ [Fig. 1(c)]. In class **2** radicals, SOC involving virtual orbitals, principally the lowest unoccupied molecular orbital (LUMO), also contributes to anisotropic exchange [Fig. 1(d)]. As a consequence, in these so-called "multiorbital" systems, the presence of heavy atoms in formally non-spin-bearing sites can enhance pseudodipolar ferromagnetic interaction terms. In this paper we present theoretical expressions for anisotropic exchange for both single- and multiorbital radicals and demonstrate the validity of our approach by using FMR and antiferromagnetic resonance (AFMR) spectroscopy to explicitly probe the consequences of substitution effects on the exchange anisotropy in **1D** (R_1/R_2 = Et/I), and **2A**•EtCN (R_2 = I), both of which contain a heavy atom substituent iodine ($n = 5$) in the basal R_2 position. Our measurements confirm that the extent of SOC due to the iodine substituent is dictated by the molecular orbitals that dominate the exchange.

In neither case does the symmetry of the SOMO permit, to first order, any spin density at the position of substitution but, in **2A**•EtCN ($R_2 = \mathrm{I}$), there is a low-lying unoccupied molecular orbital (the LUMO) that does.

II. THEORETICAL MODELS

A. Single-orbital (SOMO-SOMO) radicals

Magnetic interactions in crystalline organic radicals are typically dominated by isotropic exchange effects which are often described in terms of the two-site single-orbital Hubbard model [Fig. 1(e)]. Within this approximation, the exchange parameter, J_{ij}, defined in terms of the isotropic Heisenberg Hamiltonian, $\hat{H}_\mathrm{I} = -2J_{ij}\hat{\mathbf{S}}_i \cdot \hat{\mathbf{S}}_j$ (we use the $-2J\hat{\mathbf{S}}_1 \cdot \hat{\mathbf{S}}_2$ convention here for consistency with previous publications) [15], between two radicals on adjacent sites, i and j, is given by the expression in Eq. (1):

$$2J_{ij} = 2J_{ij}^{\mathrm{FM}} + 2J_{ij}^{\mathrm{AFM}} = 2K_{ij}^{00} - 4\left(t_{ij}^{00}\right)^2/U. \tag{1}$$

The magnitude and sign of J_{ij} depends upon (i) the intermolecular hopping integral t_{ij}^{00}, which is directly related to the SOMO-SOMO overlap; (ii) the on-site Coulomb potential U; and (iii) the electron exchange integral K_{ij}^{00} (Hund's coupling), between the two radicals. The "00" in the superscripts refer to the SOMOs associated with the two radical sites; i.e., we number orbitals at each site i and j, with "0" representing the SOMO, "1" representing the LUMO, and so on (this will become important later on when considering "multiorbital" radicals). Qualitatively, strong overlap leads to a large virtual hopping term $4(t_{ij}^{00})^2/U$, which favors AFM exchange ($-$ve J_{ij}), while FM exchange (Hund's coupling with $+$ve J_{ij}) is favored when SOMO-SOMO overlap, and hence t_{ij}^{00}, is nullified.

While the above model [Eq. (1)] provides an effective framework for rationalizing the magnetic behavior of virtually all light-atom ($n \leqslant 3$) radicals, when heavier ($n > 3$) atoms are incorporated into spin-bearing sites, as in the heavier members of the series **1A**–**1D**, SOC-driven anisotropic exchange interactions must also be considered. For structures based on isolated atomic ions, anisotropic exchange generated by the coupling of spin (**S**) and orbital (**L**) momenta may be expressed via the Hamiltonian, $\hat{H}_\mathrm{SOC} = \lambda\hat{\mathbf{L}} \cdot \hat{\mathbf{S}}$, with a magnitude set by the empirical SOC constant, λ, which grows sharply with increasing atomic number (roughly as Z^4) [31]. In molecular systems, however, the presence of multiatom and multielectron SOC contributions is such that $\hat{H}_\mathrm{SOC}$ cannot be expressed in terms of a single atomic parameter λ, or operator $\hat{\mathbf{L}}$. Instead, one must introduce an effective one-electron molecular operator $\widehat{\mathcal{L}}$, such that $\hat{H}_\mathrm{SOC} = \lambda\widehat{\mathcal{L}} \cdot \hat{\mathbf{S}}$, which may be computed within the spin-orbit mean field (SOMF) approximation [32,33]. To first order, this interaction in orbitally nondegenerate radicals mixes filled and virtual (unoccupied) orbitals to induce nonzero orbital angular momentum at the expense of the spin moment. The physical consequence of this mixing is that the spin/orbital composition of the observable magnetic moment becomes orientation dependent, which results in increased anisotropy in the g tensors of isolated selenium-based radicals compared to their sulfur counterparts [34]. In the solid state, the exchange interactions between composite spin-orbital moments are also rendered anisotropic, and may be generally described by extension of the isotropic Heisenberg Hamiltonian ($\hat{H}_\mathrm{I}$) to include anisotropic terms [Eq. (2)]:

$$\hat{H}_\mathrm{A} = -2J_{ij}\hat{\mathbf{S}}_i \cdot \hat{\mathbf{S}}_j + \mathbf{D}_{ij} \cdot \hat{\mathbf{S}}_i \times \hat{\mathbf{S}}_j + \hat{\mathbf{S}}_i \cdot \overleftrightarrow{\Gamma}_{ij} \cdot \hat{\mathbf{S}}_j. \tag{2}$$

In this expression the vector $\mathbf{D}_{ij}$ is the antisymmetric Dzyaloshinskii-Moriya (DM) term [35,36], while the symmetric tensor $\overleftrightarrow{\Gamma}_{ij}$ represents the pseudodipolar (PD) interaction. Both DM and PD effects arise from the presence of SOC interactions and may contribute to the total magnetic anisotropy given the appropriate symmetry conditions. The DM term prefers $\hat{\mathbf{S}}_i$ and $\hat{\mathbf{S}}_j$ to be canted with respect to each other and lie in the plane perpendicular to the $\mathbf{D}_{ij}$ vector, with the anisotropy field $H_\mathrm{A} \sim |\mathbf{D}_{ij}|/\mu_\mathrm{B}J_{ij}$ [not to be confused with the anisotropic Hamiltonian $\hat{H}_\mathrm{A}$ of Eq. (2)]. The PD term prefers $\hat{\mathbf{S}}_i$ and $\hat{\mathbf{S}}_j$ to be parallel (perpendicular) to the largest positive principal axis of the $\overleftrightarrow{\Gamma}_{ij}$ tensor for AFM (FM) aligned spins.

The standard microscopic description for the DM and PD terms, which we have previously applied to **1B** and **1D** ($R_1/R_2 = \mathrm{Et/Cl}$), stems from the work of Moriya [35], who considered isolated $S = \frac{1}{2}$ atomic centers and computed SOC corrections to the AFM exchange by using Eqs. (3) and (4):

$$\mathbf{D}_{ij}^{\mathrm{AFM}} = \frac{4\mathrm{i}}{U}\left\{t_{ij}^{00}\boldsymbol{C}_{ji}^{00} - \boldsymbol{C}_{ij}^{00}t_{ji}^{00}\right\}, \tag{3}$$

$$\Gamma_{ij}^{\mathrm{AFM}} = \frac{4}{U}\left\{\boldsymbol{C}_{ij}^{00} \otimes \boldsymbol{C}_{ji}^{00} + \boldsymbol{C}_{ji}^{00} \otimes \boldsymbol{C}_{ij}^{00}\right\}. \tag{4}$$

In the above two equations, the SOMO-SOMO spin-orbit hopping parameter $\boldsymbol{C}_{ij}^{00}$ is a (pseudo-) vector, with Cartesian components given in Eq. (5),

$$\left[\boldsymbol{C}_{ij}^{00}\right]_\mu = \frac{1}{2}\left\{\sum_{a\neq 0}\frac{\langle\phi_i^0|\hat{\mathcal{L}}_i^\mu|\phi_i^a\rangle}{\varepsilon_a - \varepsilon_0}t_{ij}^{a0} + \sum_{a\neq 0}t_{ij}^{0a}\frac{\langle\phi_j^a|\hat{\mathcal{L}}_j^\mu|\phi_j^0\rangle}{\varepsilon_a - \varepsilon_0}\right\}, \tag{5}$$

in which $\mu \in \{x, y, z\}$; t_{ij}^{a0} (t_{ij}^{0a}) is the hopping integral between orbital ϕ_i^a (ϕ_i^0) at radical site i and orbital ϕ_j^0 (ϕ_j^a) at site j. The index a runs over all orbitals in the summation, and $a = 0$ refers to the SOMO; ε_a and ε_0 refer to the corresponding orbital energies. The orientation and magnitude of $\boldsymbol{C}_{ij}^{00}$ completely determines the character of the magnetic anisotropy. While Moriya's approach is equally valid for organic radicals, a conceptual disadvantage of writing $\boldsymbol{C}_{ij}^{00}$ in terms of molecular operators $\widehat{\mathcal{L}}_i$ is that the energy scale for the interaction is no longer set by a single atomic λ, complicating comparison of different molecular materials. Moreover, SOC may have varied effects on different orbitals, as discussed below. In order to address this complication, we introduce the orbital-dependent weighting functions shown in Eqs. (6) and (7):

$$\mathcal{P}_\mu(a, \mathcal{E}) = \sum_{\substack{b\neq a \\ |\varepsilon_a - \varepsilon_b| \leqslant \mathcal{E}}}\left|\frac{\langle\phi_i^a|\hat{\mathcal{L}}_i^\mu|\phi_i^b\rangle}{\varepsilon_a - \varepsilon_b}\right|, \tag{6}$$

$$\mathcal{P}_\mathrm{tot}(a, \mathcal{E}) = \sum_{\substack{b\neq a \\ |\varepsilon_a - \varepsilon_b| \leqslant \mathcal{E}}}\sqrt{\sum_\mu\left(\left|\frac{\langle\phi_i^a|\hat{\mathcal{L}}_i^\mu|\phi_i^b\rangle}{\varepsilon_a - \varepsilon_b}\right|\right)^2}. \tag{7}$$

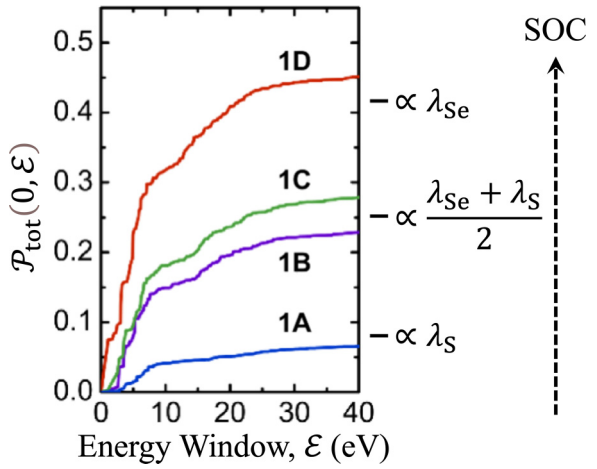

FIG. 3. Calculated weighting function, $\mathcal{P}_{tot}(0, \mathcal{E})$, for **1A**–**1D** ($R_1/R_2$ = Et/Cl) as a function of the width of the energy window $\mathcal{E}$ [15]. The limiting values of $\mathcal{P}_{tot}(0, \mathcal{E})$ appear in the same ratio as the average SOC constants for the heavy (S, Se) atoms in the molecule.

Both functions quantify the degree of first-order spin-orbit mixing of orbital ϕ_i^a with all other orbitals on the same site lying within an energy window $\mathcal{E}$. The first function, $\mathcal{P}_\mu$, describes the relative weight of SOC induced by the different Cartesian components of $\hat{\mathcal{L}}$, which, for $a = 0$, is closely related to the orientation of $\boldsymbol{C}_{ij}^{00}$ and, therefore, the character of the anisotropic exchange. The second function, $\mathcal{P}_{tot}$, quantifies the total weight of mixing, and is related to the overall scale of the SOC, analogous to λ. For example, for anisotropic exchange, the anisotropy field $H_A \propto |\boldsymbol{C}_{ij}^{00}|$ [2] and, therefore, should scale roughly as $|\mathcal{P}_{tot}(0, \mathcal{E})|^2$ in the limit $\mathcal{E} \to \infty$. Values of $\mathcal{P}_{tot}(0, \mathcal{E})$, computed at the B3LYP/def2-SV(P) level using ORCA [37], are plotted in Fig. 3 for **1A**–**1D** (R_1/R_2 = Et/Cl) [15]. As can be seen, the summation is slowly converging; consequently, large energy windows must be considered. The results indicate that the ratios of $\mathcal{P}_{tot}(0, \mathcal{E})$ values for **1A**–**1D** (R_1/R_2 = Et/Cl) converge towards those determined by the average atomic spin-orbit-coupling parameters λ of the chalcogen atoms [38] within the molecular framework. On this basis, one expects that H_A for **1B** and **1D** should be roughly in the ratio $[(\lambda_S + \lambda_{Se})/2\lambda_{Se}]^2 = 0.36$, in excellent agreement with the value found experimentally (∼0.35) [15].

B. Multiorbital (SOMO-LUMO) radicals

The multiorbital phenomenon, though relatively rare in radical-based systems [39,40], was well recognized by Anderson [41] and Goodenough [42] in the context of magnetic oxides, and their ideas were later applied to the design of charge-transfer ferromagnets [8,43]. The possible involvement of such an effect in **2A** was first indicated by electrochemical measurements and density functional theory (DFT) calculations, which revealed an unusually low-lying LUMO arising from the interaction of a carbonyl group with the π manifold of the radical [15,30]. While the π^*-acceptor orbital of the carbonyl C=O unit does not, by symmetry, perturb the a_2 SOMO, it is able to mix with the b_1 LUMO, giving rise to a small SOMO-LUMO energy gap, $\Delta\epsilon$ [Fig. 1(f)]. The presence of this low-lying LUMO, and the consequent large on-site SOMO-LUMO Hund's coupling, K_{ii}^{01}, leads to a strong FM exchange interaction through virtual hopping processes; note here that the "01" superscript and "*ii*" subscript imply on-site SOMO and LUMO coupling. The suitably modified isotropic FM exchange term is given in Eq. (8),

$$2J_{ij}^{FM} = 2K_{ij}^{00} + 2\frac{\left(t_{ij}^{01}\right)^2 + \left(t_{ij}^{10}\right)^2}{(V+\Delta\epsilon)^2 - \left(K_{ii}^{01}\right)^2} 2K_{ii}^{01}, \tag{8}$$

where the on-site Coulomb repulsion term V ($<U$) refers to two electrons in different orbitals on the same molecule, while the t_{ij}^{01} (t_{ij}^{10}) describe hopping processes between the SOMO (superscript "0") and LUMO (superscript "1") on adjacent sites i and j.

An understanding of the magnetic anisotropy of multiorbital radicals such as **2A** can be developed in a similar manner, by modification [44] of Moriya's standard description, to include anisotropic SOC corrections to the multiorbital FM exchange. Accordingly, the second and third terms in Eq. (2) must be redefined by including the expressions provided in Eqs. (9) and (10):

$$\mathbf{D}_{ij}^{FM} = -2i\left\{\frac{\boldsymbol{C}_{ij}^{01} t_{ji}^{10} - t_{ij}^{10}\boldsymbol{C}_{ji}^{01}}{(V+\Delta\epsilon)^2 - \left(K_{ii}^{01}\right)^2}\right\} K_{ii}^{01}, \tag{9}$$

$$\Gamma_{ij}^{FM} = -2\left\{\frac{\boldsymbol{C}_{ij}^{01} \otimes \boldsymbol{C}_{ji}^{10} + \boldsymbol{C}_{ji}^{01} \otimes \boldsymbol{C}_{ij}^{10}}{(V+\Delta\epsilon)^2 - \left(K_{ii}^{01}\right)^2}\right\} K_{ii}^{01}. \tag{10}$$

These are distinguished from Moriya's conventional anisotropic exchange terms by the superscript "FM". The interorbital (SOMO-LUMO) SOC-mediated hopping $\boldsymbol{C}_{ij}^{01}$ is then given by Eq. (11):

$$\left[\boldsymbol{C}_{ij}^{01}\right]_\mu = \frac{1}{2}\left\{\sum_{a\neq 0}\frac{\langle\phi_i^0|\hat{\mathcal{L}}_i^\mu|\phi_i^a\rangle}{\varepsilon_a - \varepsilon_0} t_{ij}^{a1} + \sum_{a\neq 1} t_{ij}^{0a}\frac{\langle\phi_j^a|\hat{\mathcal{L}}_j^\mu|\phi_j^1\rangle}{\varepsilon_a - \varepsilon_1 + V}\right\}. \tag{11}$$

It is important to note from Eq. (11) that, in contrast to $\boldsymbol{C}_{ij}^{00}$ defined in Eq. (5), the value of $\boldsymbol{C}_{ij}^{01}$ depends on SOC effects in both the SOMO and the LUMO, through the first and second terms, respectively. As a result, while the magnitude of $\boldsymbol{C}_{ij}^{00}$ is related only to $\mathcal{P}_{tot}(0, \mathcal{E})$, the interorbital SOC terms $\boldsymbol{C}_{ij}^{01}$ scale with both $\mathcal{P}_{tot}(0, \mathcal{E})$ and $\mathcal{P}_{tot}(1, \mathcal{E})$. To illustrate this point, Fig. 4 displays the values of these two terms for **2A** (R_2 = F, Cl, Br, I), computed at the B3LYP/def2-SV(P) level [37], which reveal an important distinction between the behavior of the SOMO and LUMO [15]. As may be seen in Fig. 1(d), the a_2 SOMO for these radicals contains a vertical nodal plane at the R_2 position and, as a consequence, SOC corrections are independent of both the R_2 group and the C = O moiety: for large $\mathcal{E}$, $\mathcal{P}_{tot}(0, \mathcal{E})$ converges to the same value in **2A** for all substituents at the R_2 position [Fig. 4(a)]. By contrast, the b_1 LUMO [Fig. 1(d)], which possesses nonzero density at the R_2 position, gives rise to spin-orbit effects that scale roughly with

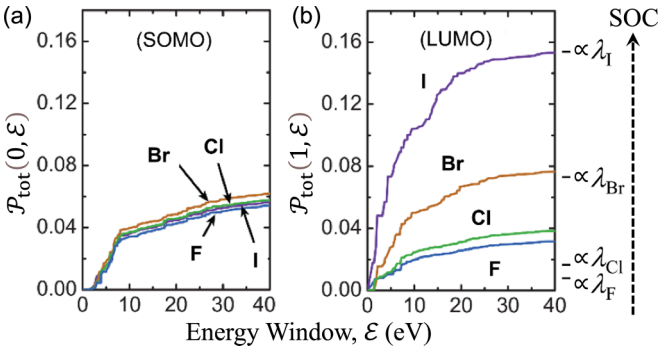

FIG. 4. Calculated weighting functions (a) $\mathcal{P}_{\rm tot}(0,\mathcal{E})$ for the SOMO and (b) $\mathcal{P}_{\rm tot}(1,\mathcal{E})$ for the LUMO of **2A** with R_2 = F, Cl, Br, I, as a function of the width of the energy window $\mathcal{E}$ [15].

the spin-orbit constant λ for R_2 (= F, Cl, Br, I), as quantified by $\mathcal{P}_{\rm tot}(1,\mathcal{E})$ [Fig. 4(b)].

III. EXPERIMENTAL METHODS

In order to assess the influence of both single- and multiorbital contributions to the anisotropic exchange in class **1** and **2** radicals, a series of FMR and AFMR experiments were, respectively, carried out on **1D** (R_1/R_2 = Et/I) and **2A** (R_2 = I), both of which possess a heavy atom substituent (iodine) in the basal position; samples were prepared as previously described [30,45]. The results were then compared to those previously published for **1D** (R_1/R_2 = Et/Cl) [18,19] and **2A** (R_2 = F) [45], each of which contains a lighter halogen at the R_2 position. With the exception of **1D** (R_1/R_2 = Et/Cl), for which FMR studies were performed previously on an oriented single crystal [18,19,46,47], all measurements were made on ∼50 mg constrained powders using a broadband homodyne spectrometer in the electron magnetic resonance (EMR) facility at the U.S. National High Magnetic Field Laboratory (NHMFL) [48]. This is a transmission-type spectrometer, employing solid-state microwave sources (Virginia Diodes Inc., USA) capable of generating frequencies in the 25–600 GHz range that are propagated to/from the sample via oversized cylindrical light pipes. A sweepable magnetic field is generated using a 15/17 T superconducting magnet (Oxford Instruments plc, UK), which is outfitted with a helium flow cryostat. The frequency- and temperature-dependent FMR and AFMR powder spectra, respectively shown in Figs. 5(a) and 5(b), were collected in derivative mode using field modulation in combination with phase-sensitive lock-in detection via a broadband hot electron InSb bolometer (QMC Instruments Ltd, UK). The spectra are thus plotted as the derivative of the transmission signal intensity, I, with respect to the applied magnetic field $H_{\rm app}$, i.e., $\mathrm{d}I/\mathrm{d}H_{\rm app}$. The resonance positions in each trace are determined from the turning points of the spectra (see insets to Fig. 5): the uniaxial system **1D** (R_1/R_2 = Et/I) results in two such turning points at the leading and trailing edges of the powder averaged spectrum, corresponding, respectively, to microcrystals with $H_{\rm app}$ parallel and perpendicular to the magnetic easy (c) axis [see Fig. 2(a)]. Meanwhile, orthorhombic **2A**•EtCN (R_2 = I) displays three turning points, corresponding to the easy, intermediate, and hard directions. In both sets of spectra, all turning points can be observed, except for the two lowest frequencies (25 and 51 GHz) for **2A**•EtCN (R_2 = I).

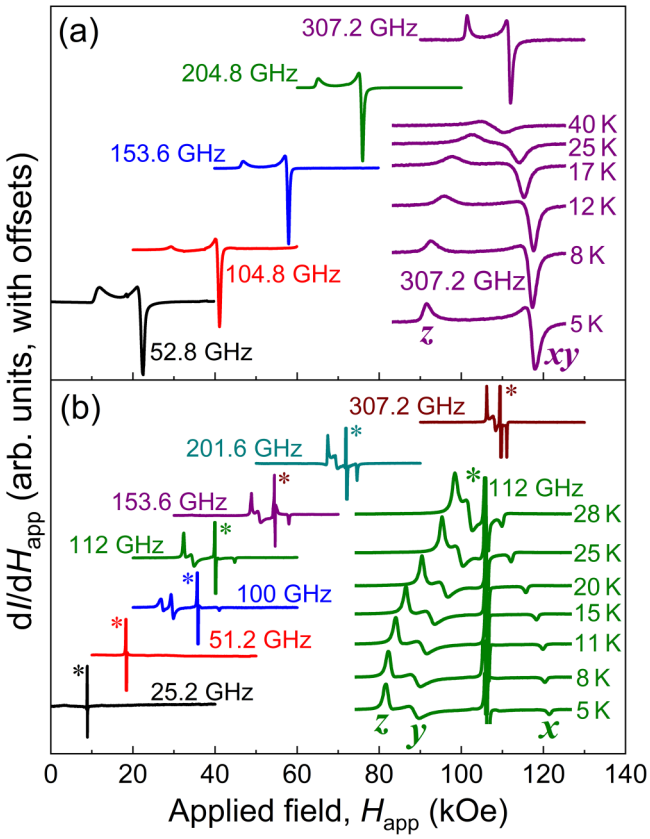

FIG. 5. (a) Normalized FMR spectra of **1D** (R_1/R_2 = Et/I) and (b) AFMR spectra of **2A**•EtCN (R_2 = I), shown both as a function of frequency (at 5 K) and temperature (see lower-right insets, with horizontal scale expanded); the frequencies and temperatures are indicated in the plots. The two observable turning points in (a) correspond to the easy-axis ($\mathbf{H}_{\rm app}//z$ or c) and hard-plane ($\mathbf{H}_{\rm app}//xy$ or ab) components of the spectra, as expected for a uniaxial system. The three features labeled x, y, and z in (b) correspond to the spectral components of an orthorhombic spin-canted antiferromagnet, two of which vanish below 60 GHz (see main text and Fig. 6). A noticeable g = 2.00 impurity signal (∗) can also be observed, most likely arising from solvent loss upon grinding the polycrystalline material. Although this signal appears quite strong in derivative mode, the double-integrated area accounts for less than 1% of the total spectral density and can thus be neglected in the analysis.

IV. RESULTS

The resonance conditions for the spectra shown Fig. 5 can be determined by solving the semiclassical Landau-Lifshitz equation of motion for a sublattice of net magnetization **M** [49]:

$$\frac{\partial \mathbf{M}^{\pm}}{\partial t} = \gamma \mathbf{M}^{\pm} \times \mathbf{H}_{\rm eff}, \tag{12}$$

where any effects from damping, which contribute to the overall line shape, have been neglected. Note here that, in

AFMR, the magnetizations of the antialigned sublattices, $\mathbf{M}^+$ and $\mathbf{M}^-$, are denoted in the superscript; this distinction is not necessary in FMR. Here, the gyromagnetic ratio is given by $\gamma = g\mu_B/\hbar$, with the g value being constrained to that of the free electron. The effective field, $\mathbf{H}_{\text{eff}}$, considers all of the magnetic contributions to the free energy density F:

$$\mathbf{H}_{\text{eff}} = \nabla_{\mathbf{M}_{x,y,z}} F, \tag{13}$$

where, for a uniaxial system (such as **1D**) in an applied magnetic field [50],

$$F = -\mathbf{M}\cdot\mathbf{H}_{\text{app}} - H_A|\mathbf{M}|\cos^2\theta_M. \tag{14}$$

Here, $\mathbf{H}_{\text{app}}$ is the applied magnetic field vector, while the anisotropy field is parametrized by H_A, with θ_M being the angle between the magnetization $\mathbf{M}$ and the easy axis (i.e., $\theta_M = 0^\circ$ and 90° correspond, respectively, to the easy and hard magnetization directions). With this notation, the free energy for the orthorhombic antiferromagnet **2A**•EtCN (R_2 = I) can conveniently be expressed as [50,51]

$$F = -\mathbf{H}_{\text{app}}\cdot(\mathbf{M}^+ + \mathbf{M}^-) - \frac{H_{\text{ex}}}{|\mathbf{M}|}(\mathbf{M}^+\cdot\mathbf{M}^-) - \frac{H_{A_2}}{|\mathbf{M}|}\mathbf{M}_z^+\mathbf{M}_z^- - \frac{H_{A_1}}{|\mathbf{M}|}\mathbf{M}_y^+\,\mathbf{M}_y^-, \tag{15}$$

where $|\mathbf{M}| = |\mathbf{M}^+| = |\mathbf{M}^-|$. The degree of orthorhombicity is defined in terms of the anisotropy field components given by $\mathbf{H}_A = (0,\ H_{A_1},\ H_{A_2})$, along the x, y, and z directions, with x corresponding to the easy axis in the case of **2A**•EtCN (R_2 = I), while the antiferromagnetic exchange field strength between magnetic sublattices is parametrized by H_{ex}.

To determine the FMR/AFMR magnetic field positions from the above expressions, a time-dependent harmonic solution of the form $M(t) = M_0 e^{i\omega t}$ can be assumed, where M_0 is given by the magnitude of the sublattice magnetization and ω denotes angular frequency. First, considering the uniaxial ferromagnetic system, **1D**, whose degrees of freedom are described in Eq. (14), the solution to Eq. (12) in terms of the anisotropy field, H_A, gives the following resonance conditions when the applied field, H_{app}, is parallel to the easy axis and the hard plane [respectively, the c axis and ab plane in Fig. 2(a)] [18]:

$$\text{Easy axis:}\ \ \omega = \gamma(H_{\text{app}} + H_A),$$
$$\text{Hard plane:}\ \ \omega = \gamma[H_{\text{app}}(H_{\text{app}} - H_A)]^{1/2}. \tag{16}$$

From this, the resonance positions determined from the spectra shown in Fig. 5(a) can be used to constrain the anisotropy field, H_A = 7.86 kOe, as shown in Fig. 6(a).

As more spectral features can be resolved for the SC-AFM system **2A**•EtCN (R_2 = I) in Fig. 5(b), the resonance conditions are given by the following three solutions to Eq. (12) [51]:

$$\text{Hard axis:}\ \ \omega = \gamma\left[H_{\text{app}}^2 + 2H_{\text{ex}}H_{A_2}\right]^{1/2},$$
$$\text{Intermediate axis:}\ \ \omega = \gamma\left[H_{\text{app}}^2 + 2H_{\text{ex}}H_{A_1}\right]^{1/2},$$
$$\text{Easy axis:}\ \ \omega = \gamma\left[H_{\text{app}}^2 - 2H_{\text{ex}}H_{A_1}\right]^{1/2}, \tag{17}$$

where the easy-axis fit provides a constraint on the spin-flop field, $H_{\text{SF}} = \sqrt{2H_{\text{ex}}H_{A_1}}$, defined as the field at which the spontaneous magnetization flips from the easy axis to the intermediate direction [52], manifested as a discontinuity in the frequency dependence seen in Fig. 6(b). From previous magnetization experiments [30], fixing H_{ex} = 350 kOe yields H_{A_1} = 610 Oe and H_{A_2} = 740 Oe from the fits in Fig. 6(b). This parametrization gives a spin-flop field of H_{SF} = 20.6 kOe, which agrees well with the magnetization measurements that give H_{SF} = 21 kOe at 28 K [30]. Contributions from canting were neglected, as this did not improve the fit to the resonance positions, again consistent with previous magnetization measurements [30].

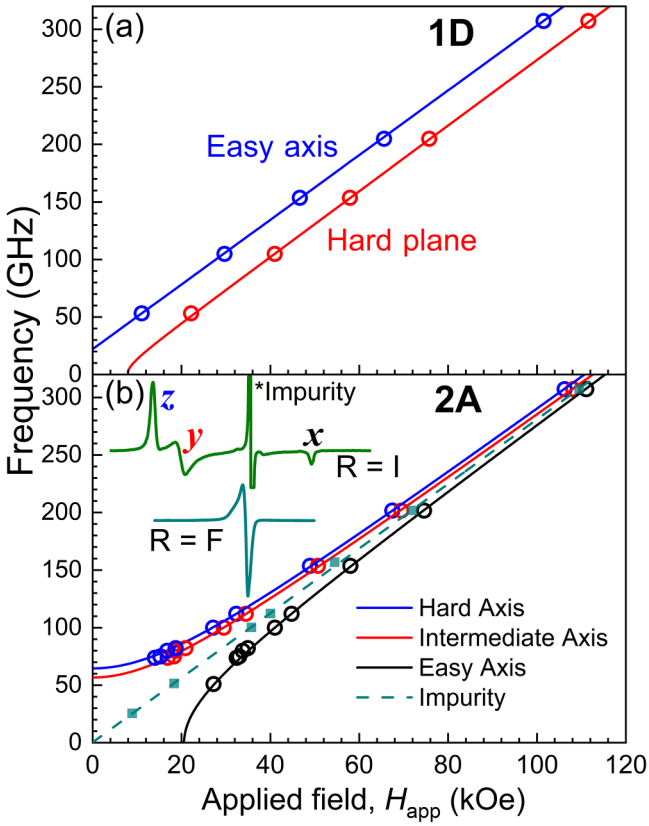

FIG. 6. Resonance frequency versus field plot for the different spectral components (open circles) deduced from Fig. 5 for (a) **1D** (R_1/R_2 = Et/I) and (b) **2A**•EtCN (R_2 = I). The solid curves are fits to the data according to (a) Eq. (16) and (b) Eq. (17), from which the anisotropy fields, H_A, are determined. The cyan dashed line and solid square data points in (b) correspond to the g = 2.00 impurity signal (∗). The intercept on the abscissa at 20.6 kOe in (b) gives the spin-flop field H_{SF}, while the inset shows a comparison between **2A** (R_2 = F) [45] and **2A**•EtCN (R_2 = I) at 112 GHz. This demonstrates a clear augmentation of the anisotropy upon introducing a heavier substituent at the R_2 position.

These results, when coupled with those obtained from previous measurements on **2A** (R_2 = F), allow for a comparison between the single-orbital (**1D**) and multiorbital (**2A**) systems. To this end, the anisotropy fields extracted from the fits given by Eqs. (16) and (17), along with other relevant quantities, are compiled in Table I.

Considering first the two isostructural ferromagnetic systems, **1D** (R_1 = Et, R_2 = Cl, I), it may be seen that, upon incorporation of a heavier halogen at R_2, H_A decreases by

TABLE I. Magnetic parameters for **1D** (R_1 = Et, R_2 = Cl and I), **2A** (R_2 = F), and **2A**•EtCN (R_2 = I).

1D	Space group	H_A (kOe)	H_c (kOe)	T_C (K)		
R_2 = Cl	$P\bar{4}2_1m$	8.20[a]	1.37[b]	17.0[b]		
R_2 = I	$P\bar{4}2_1m$	7.86	0.39[c]	10.5[c]		
2A	Space group	H_{A_1}(Oe)	H_{A_2}(Oe)	H_{ex} (kOe)	H_c (Oe)	T_N (K)
R_2 = F	$Cmc2_1$	200[d]	–	250[d]	290[d]	13.0[d]
R_2 = I	*Pnma*	610	740	350[e]	1060[e]	35.0[e]

[a]References [18,19].
[b]Reference [16].
[c]References [22,23].
[d]References [28,45].
[e]Reference [30].

only ∼4%; this is in spite of somewhat larger decreases in both H_c and T_C. However, a very different trend is found for the SCAFM systems **2A**, where a rather large increase in the exchange anisotropy is seen upon substitution of I for F. Not only does the magnitude of the anisotropy increase by more than a factor of 3 but, for the iodo derivative, all three components are resolved in the AFMR spectra. This is demonstrated in the inset to Fig. 6(b), which compares the spectral features obtained at 112 GHz for **2A**•EtCN (R_2 = I) with those for **2A** (R_2 = F) [45], where the anisotropy is barely resolvable. It is important to note that the exchange field (H_{ex}) makes a non-negligible contribution to the resonant field position [see Eq. (17)], and that these fields are appreciably different for the two compounds. This is due to the fact that the two radicals are not isostructural; they crystallize in different space groups, i.e., $Cmc2_1$ (**2A** with R_2 = F) and *Pnma* (**2A**•EtCN with R_2 = I), with the latter being more favorable for a larger interstack exchange, which ultimately gives rise to a 40% stronger H_{ex} (350 kOe versus 250 kOe), as seen in Table I. A more detailed discussion regarding SOMO-SOMO overlap and the role of slippage between the neighboring π stacks is outlined in Ref. [15].

V. DISCUSSION

The results shown in Table I can be satisfactorily interpreted in terms of the calculated SOMO $\mathcal{P}_{tot}(0, \mathcal{E})$ and LUMO $\mathcal{P}_{tot}(1, \mathcal{E})$ weighting functions derived in Sec. II. Before doing so, however, we note that spin-spin dipolar interactions and demagnetization effects can be ruled out as explanations for the observed magnetic anisotropy, as we have discussed elsewhere [15,18,19]. We thus conclude that the overwhelming contribution to the anisotropy is from SOC, and that the trends arising in the anisotropic exchange (i.e., the H_A values in Table I) can be explained via consideration of the weighting functions displayed in Figs. 3 and 4. For the sake of this discussion, any contributions from the DM interaction are neglected as they were not required to constrain the anisotropy fields deduced from either the FMR or AFMR measurements. As such, the sole contribution to the anisotropic exchange originating from SOC is given by the pseudodipolar exchange term [15]. From this, the anisotropy in zero applied magnetic field can be approximated by $g\mu_B H_A \propto \mathrm{Tr}[\Gamma_{ij}^{AFM}]$ for **1D** and $g\mu_B H_A \propto \mathrm{Tr}[\Gamma_{ij}^{FM}]$ for **2A**, which are, respectively, outlined in Eqs. (4) and (10).

Focusing first on **1D**, where the exchange anisotropy is dominated by the SOMO-SOMO spin-orbit hopping parameter $\boldsymbol{C}_{ij}^{00}$, given in Eq. (5), there is a dramatic increase seen in $\mathcal{P}_{tot}(0, \mathcal{E})$ occasioned by the sequential replacement of sulfur by its heavier congener selenium. These changes are also manifest in the experimentally observed exchange anisotropies. However, by virtue of the nodal plane which bisects the a_2 SOMO of the molecule, there can be no appreciable spin density at the R_2 position. Accordingly, comparison of the FMR results for **1D** (R_1 = Et, R_2 = Cl, I) indicate that substituents at the basal R_2 position have no influence on SOC and, ultimately, lead to no impact on the anisotropic exchange between neighboring molecules. The converse is true for **2A**. While the symmetry of the SOMO remains the same as for **1D**, the LUMO, which lies just 0.2−0.4 eV above the SOMO, displays b_1 symmetry and has a rather sizable density at the R_2 position. As a result, the weighting function $\mathcal{P}_{tot}(1, \mathcal{E})$ calculated in Fig. 4(b) varies drastically with the atomic number (Z) of the substituent at the R_2 position, scaling roughly as λ_{R_2} for a large enough energy window. As such, an enhanced LUMO-mediated anisotropic exchange in **2A**•EtCN (R_2 = I) compared to **2A** (R_2 = F) is fully anticipated.

In principle, the significant increase of magnetic anisotropy in **2A**•EtCN (R_2 = I) compared with **2A** (R_2 = F) could be attributed to differences in molecular packing rather than enhancement of SOC, since the two materials are not isostructural. However, symmetry considerations and explicit *ab initio* calculations of $\boldsymbol{C}_{ij}$ point to SOC enhancement [30]. It may first be noted that both materials display a net canted moment, which uniquely restricts the possible antiferromagnetic ordering patterns in both cases: spins within the same π stack must be ferromagnetically aligned by symmetry. The primary effect of SOC on the SOMO and LUMO of **2A**, both of which are π orbitals, is to mix them with σ orbitals [15,53], thus inducing an orbital moment in the molecular plane. This has the following effects: (i) the component of $\boldsymbol{C}_{ij}$ perpendicular to the plane of the molecule is suppressed, and (ii) the anisotropic coupling between any two planar molecules that lie in the same plane is also suppressed.

Although **2A** (R_2 = F) and **2A**•EtCN (R_2 = I) are not isostructural, it follows that the anisotropic exchange is dominated by the interactions along the π-stacking direction in both materials. For **2A** (R_2 = I), inversion symmetry further restricts the spin-orbit-mediated SOMO-SOMO hopping so

that $\boldsymbol{C}_\pi^{00}$ is strictly zero. As a result, the large anisotropy field H_A (Table I) for **2A**•EtCN (R_2 = I) can only arise from Γ_π^{FM}, through an enhanced SOMO-LUMO hopping term $|\boldsymbol{C}_\pi^{01}|^2$ prompted by the heavy iodine substituent. Due to the sign of Γ_π^{FM}, this interaction provides each π stack (which is ordered ferromagnetically within the stack) with an easy-axis, which was previously estimated [30] to lie near the crystallographic a axis. This is fully compatible with the observed AFMR modes, and the previous *ab initio* estimates of $H_A = 500 - 700$ Oe, which are in excellent agreement with the value observed here. In contrast, for **2A** (R_2 = F), both Γ_π^{FM} and Γ_π^{AFM} may be finite. However, a significant contribution from Γ_π^{FM} may be largely ruled out on the basis of the observed easy-plane anisotropy. In this material, the π-stacked molecules form a 2D brick-wall grid of sites in the ab plane related to each other by translation (C centering). If Γ_π^{FM} were dominant, it would provide each 2D layer with an easy axis, given that the spins within each layer are ordered ferromagnetically. By contrast, a dominant Γ_π^{AFM} acting between ferromagnetically aligned spins produces an easy plane. The latter scenario is overall more compatible with the observed AFMR modes. Moreover, inspection of Eqs. (4) and (10) suggests that Γ_π^{FM} should tend to be weaker than Γ_π^{AFM} by a factor of roughly $K_{ii}^{01}/U \sim 0.1$. The latter coupling should therefore tend to dominate when both are present. This same observation also explains the order of magnitude difference in H_A between **2A**•EtCN (R_2 = I) and **1D** materials. The net conclusion is that the incorporation of the heavy iodine substituent enhances Γ_π^{FM} in **2A** to a similar degree as incorporation of selenium enhances Γ_π^{AFM} in **1D**.

VI. CONCLUSIONS

We have discussed the contribution of heavy-atom substituents to the overall SOC interaction in two classes of organic radical magnets. As shown by the FMR and AFMR results, substitution of the heavy-atom iodine at the R_2 position in the "single-orbital" radical **1D** effects essentially no variation in the anisotropic exchange, while the same substitution in the "multiorbital" radical **2A** significantly augments the magnetic anisotropy. These results are supported by the incorporation of multiorbital exchange models via DFT calculations. In so doing, we demonstrate the role of the SOMO-LUMO gap in dictating the nature of the anisotropic exchange between neighboring radical molecules.

ACKNOWLEDGMENTS

This work was supported by the Office of Naval Research – Global (Grant No. N62909-23-1-2079) and the Natural Sciences and Engineering Council of Canada. Work performed at the NHMFL is supported the NSF (Grants No. DMR-1644779 and No. DMR-2128556) and the State of Florida.

[1] M. Tamura, Y. Nakazawa, D. Shiomi, K. Nozawa, Y. Hosokoshi, M. Ishikawa, M. Takahashi, and M. Kinoshita, Chem. Phys. Lett. **186**, 401 (1991).
[2] R. Chiarelli, M. A. Novak, A. Rassat, and J. L. Tholence, Nature (London) **363**, 147 (1993).
[3] T. Sugawara, M. Matushita, A. Izuoka, N. Wada, N. Takeda, and M. Ishikawa, J. Chem. Soc., Chem. Commun. **1994**, 1723 (1994).
[4] T. Nogami, T. Ishida, H. Tsuboi, H. Yoshikawa, H. Yamamoto, M. Yasui, F. Iwasaki, H. Iwamura, N. Takeda, and M. Ishikawa, Chem. Lett. **24**, 635 (1995).
[5] S. Nakatsuji, H. Morimoto, H. Anzai, J. Kawashima, K. Maeda, M. Mito, and K. Takeda, Chem. Phys. Lett. **296**, 159 (1998).
[6] P. Day, Nature (London) **363**, 113 (1993).
[7] A. J. Banister, N. Bricklebank, I. Lavender, J. M. Rawson, C. I. Gregory, B. K. Tanner, W. Clegg, M. R. J. Elsegood, and F. Palacio, Angew. Chem. **108**, 2648 (1996).
[8] W. Fujita and K. Awaga, Chem. Phys. Lett. **388**, 186 (2004).
[9] W. Fujita, Dalton Trans. **44**, 903 (2015).
[10] J. M. Hawkins, A. Meyer, T. A. Lewis, S. Loren, and F. J. Hollander, Science **252**, 312 (1991).
[11] A. W. Cordes, R. C. Haddon, and R. T. Oakley, Phosphorus, Sulfur, Silicon Relat. Elem. **179**, 673 (2004).
[12] A. A. Leitch, J. L. Brusso, K. Cvrkalj, R. W. Reed, C. M. Robertson, P. A. Dube, and R. T. Oakley, Chem. Commun. **2007**, 3368 (2007).
[13] C. M. Robertson, D. J. T. Myles, A. A. Leitch, R. W. Reed, B. M. Dooley, N. L. Frank, P. A. Dube, L. K. Thompson, and R. T. Oakley, J. Am. Chem. Soc. **129**, 12688 (2007).
[14] L. Beer, J. L. Brusso, R. C. Haddon, M. E. Itkis, A. A. Leitch, R. T. Oakley, R. W. Reed, and J. F. Richardson, Chem. Commun. **2005**, 1543 (2005).
[15] S. M. Winter, S. Hill, and R. T. Oakley, J. Am. Chem. Soc. **137**, 3720 (2015).
[16] C. M. Robertson, A. A. Leitch, K. Cvrkalj, R. W. Reed, D. J. T. Myles, P. A. Dube, and R. T. Oakley, J. Am. Chem. Soc. **130**, 8414 (2008).
[17] C. M. Robertson, S. M. Winter, J. A. K. Howard, M. R. Probert, and R. T. Oakley, Chem. Commun. **57**, 10238 (2021).
[18] S. M. Winter, S. Datta, S. Hill, and R. T. Oakley, J. Am. Chem. Soc. **133**, 8126 (2011).
[19] S. M. Winter, R. T. Oakley, A. E. Kovalev, and S. Hill, Phys. Rev. B **85**, 094430 (2012).
[20] K. Thirunavukkuarasu, S. M. Winter, C. C. Beedle, A. E. Kovalev, R. T. Oakley, and S. Hill, Phys. Rev. B **91**, 014412 (2015).
[21] A. A. Leitch, K. Lekin, S. M. Winter, L. E. Downie, H. Tsuruda, J. S. Tse, M. Mito, S. Desgreniers, P. A. Dube, S. Zhang, Q. Liu, C. Jin, Y. Ohishi, and R. T. Oakley, J. Am. Chem. Soc. **133**, 6051 (2011).
[22] K. Lekin, K. Ogata, A. Maclean, A. Mailman, S. M. Winter, A. Assoud, M. Mito, J. S. Tse, S. Desgreniers, N. Hirao, P. A. Dube, and R. T. Oakley, Chem. Commun. **52**, 13877 (2016).
[23] K. Irie, K. Shibayama, M. Mito, S. Takagi, M. Ishizuka, K. Lekin, and R. T. Oakley, Phys. Rev. B. **99**, 014417 (2019).
[24] X. Yu, A. Mailman, P. A. Dube, A. Assoud, and R. T. Oakley, Chem. Commun. **47**, 4655 (2011).

[25] C. Climent, S. Vela, J. Jornet-Somoza, and M. Deumal, Phys. Chem. Chem. Phys. **21**, 12184 (2019).
[26] J. W. L. Wong, A. Mailman, S. M. Winter, C. M. Robertson, R. J. Holmberg, M. Murugesu, P. A. Dube, and R. T. Oakley, Chem. Commun. **50**, 785 (2014).
[27] A. Mailman, J. W. L. Wong, S. M. Winter, R. C. M. Claridge, C. M. Robertson, A. Assoud, W. Yong, E. Steven, P. A. Dube, J. S. Tse, S. Desgreniers, R. A. Secco, and R. T. Oakley, J. Am. Chem. Soc. **139**, 1625 (2017).
[28] A. Mailman, S. M. Winter, X. Yu, C. M. Robertson, W. Yong, J. S. Tse, R. A. Secco, Z. Liu, P. A. Dube, J. A. K. Howard, and R. T. Oakley, J. Am. Chem. Soc. **134**, 9886 (2012).
[29] X. Yu, A. Mailman, K. Lekin, A. Assoud, C. M. Robertson, B. C. Noll, C. F. Campana, J. A. K. Howard, P. A. Dube, and R. T. Oakley, J. Am. Chem. Soc. **134**, 2264 (2012).
[30] A. Mailman, S. M. Winter, J. W. L. Wong, C. M. Robertson, A. Assoud, P. A. Dube, and R. T. Oakley, J. Am. Chem. Soc. **137**, 1044 (2015).
[31] D. Dai, H. Xiang, and M.-H. Whangbo, J. Comput. Chem. **29**, 2187 (2008).
[32] B. A. Hess, C. M. Marian, U. Wahlgren, and O. Gropen, Chem. Phys. Lett. **251**, 365 (1996).
[33] F. Neese, J. Chem. Phys. **122**, 034107 (2005).
[34] A. V. Pivtsov, L. V. Kulik, A. Y. Makarov, and F. Blockhuys, Phys. Chem. Chem. Phys. **13**, 3873 (2011).
[35] T. Moriya, Phys. Rev. **120**, 91 (1960).
[36] I. Dzyaloshinsky, J. Phys. Chem. Solids **4**, 241 (1958).
[37] F. Neese, Wiley Interdiscip. Rev.: Comput. Mol. Sci. **2**, 73 (2012).
[38] M. Blume and R. E. Watson, Proc. R Soc. Lond. A **271**, 565 (1963).
[39] R. Kumai, M. M. Matsushita, A. Izuoka, and T. Sugawara, J. Am. Chem. Soc. **116**, 4523 (1994).
[40] J. Nakazaki, Y. Ishikawa, A. Izuoka, and T. Sugawara, and Y. Kawada, Chem. Phys. Lett. **319**, 385 (2000).
[41] P. W. Anderson, Phys. Rev. **115**, 2 (1959).
[42] J. B. Goodenough, J. Phys. Chem. Solids **6**, 287 (1958).
[43] R. Seshadri, A. Rastogi, S. V. Bhat, S. Ramasesha, and C. N. R. Rao, Solid State Commun. **85**, 971 (1993).
[44] T. Yildirim, A. B. Harris, A. Aharony, and O. Entin-Wohlman, Phys. Rev. B **52**, 10239 (1995).
[45] S. M. Winter, A. Mailman, R. T. Oakley, K. Thirunavukkuarasu, S. Hill, D. E. Graf, S. W. Tozer, J. S. Tse, M. Mito, and H. Yamaguchi, Phys. Rev. B **89**, 214403 (2014).
[46] M. Mola, S. Hill, P. Goy, and M. Gross, Rev. Sci. Instrum. **71**, 186 (2000).
[47] S. Takahashi and S. Hill, Rev. Sci. Instrum. **76**, 023114 (2005).
[48] A. Hassan, L. Pardi, J. Krzystek, A. Sienkiewicz, P. Goy, M. Rohrer, and L.-C. Brunel, J. Magn. Reson. **142**, 300 (2000).
[49] M. Date, J. Phys. Soc. Japan **16**, 1337 (1961).
[50] A. G. Gurevich and G. A. Melkov, *Magnetization Oscillations and Waves* (CRC Press, Boca Raton, FL, 1996).
[51] J. M. Rawson, A. Alberola, H. El-Mkami, and G. M. Smith, J. Phys. Chem. Solids **65**, 727 (2004).
[52] R. L. Carlin, *Magnetochemistry* (Springer, Berlin, 1986).
[53] S. M. Winter, K. Riedl, and R. Valentí, Phys. Rev. B **95**, 060404(R) (2017).